Research Article

Simple synthesis of gold-decorated silica nanoparticles by in situ precipitation method with new plasmonic properties

Lizbet León Félix[1] · Joaquin Martinez Porcel[2] · Fermín Fidel Herrera Aragón[1] · David Gregorio Pacheco-Salazar[1] · Marcelo Henrique Sousa[3]

Abstract

We describe a simple method for the preparation of gold-decorated silica (SiO_2) nanoparticles (NPs) by the in situ precipitation method using simple BH_4^- ions reduction as a procedure, where BH_4^- ions are adsorbed onto PEI-functionalized SiO_2 NPs for stabilizing and reducing gold ions onto PEI-SiO_2 surface in water under ambient conditions. The result was 3-nm gold nanoshell NPs attached to SiO_2 core (~ 75 nm) with a surface plasmon resonance (SPR) at ~ 680 nm. SPR band is associated with Au NP aggregates that arise from strong interparticle interaction. This is an alternative to the gold-seeding methods and the use of anionic gold species for the obtention of gold-decorated SiO_2 NPs with an important red-shift in UV–Vis absorption and with potential applications in biosensors and photothermal therapy.

Keywords Gold · Decorated · PEI-coated silica · Polyethyleneimine · Red-shift · Plasmonic

1 Introduction

Core–shell engineered nanostructures are good candidates for the building of new materials with controlled properties of importance in several technological applications [1]. In particular, gold nanoparticles (AuNPs) in hollow gold-shell configuration exhibit unique physical–chemical characteristics, low toxicity, and optical properties due to AuNPs. Furthermore, the synthesis of gold nanoshells NPs with various dimensions and shapes presents us the possibility of obtaining metallic nanoshells with SPR band in the near-infrared ranges. These are of considerable interest by a wide range of possible applications in fluorescent sensors [2], biosensors [3], photothermal therapy [4, 5], biomedical imaging [6], or drug carriers for cancer treatment [7]. The surface features directly affect its optical response which is key to these applications and especially in photothermal therapy which converts light into local heat (hyperthermia) that can kill cancer cells [8].

In fact, AuNPs can absorb or emit different wavelengths with responses ranging from the visible to the infrared region due to the in-phase resonant oscillation of free conduction band electrons by interacting with the electromagnetic fields, generate the surface plasmon resonance (SPR) [9, 10], very useful for different applications. The position, intensity, and shape of the SPR band depend on the size and size distribution of AuNPs, morphology, shape or geometry, the inter-particle distances, the polarization of the incident light [11], the dielectric constant of the surrounding medium around the NPs, and interparticle interaction [10–13] which are important parameters to define their plasmonic properties.

Therefore, we provide an insight into the sensitivity of SPR toward the above parameters in the following few reports. The position of absorption maximum is also

✉ Lizbet León Félix | [1]Laboratorio de Películas Delgadas, Escuela Profesional de Física, Universidad Nacional de San Agustín de Arequipa, Av. Independencia s/n, Arequipa, Perú. [2]Instituto de Investigaciones Científicas Teóricas Y Aplicadas (INIFTA), Universidad Nacional de La Plata, Diag 113 y 64, CP 1900 La Plata, Argentina. [3]Green Nanotechnology Group, Faculty of Ceilandia, University of Brasilia, Brasília, DF CEP 72220-900, Brazil.

affected by decreasing the particle size. However, as a modification to the Mie theory for small metal particles, the dielectric function is assumed to become intrinsic size effects (are mainly governed by their size, shape, composition, crystallinity, and structure) [10] dependent rendering a size-dependent absorption cross-section, and the underlying relaxation mechanisms, that does not distinguish the dephasing of the collective electron motion and are directly related to the width of the plasmon resonance [13]. Solid spherical Au NPs with low polydispersity and small diameters (2–5 nm) are well known to exhibit a single SPR band between 510 and 570 nm [14, 15]. Otherwise, when the particle size increases, the absorption band exhibits a red-shift and a band broadening that can upsurge mainly from radiative losses (the mode cannot be trapped in the particle and coupled to freely propagating light) [13]. Moreover, that the is decrease of the interparticle distance in a system of AuNPs leads to a much stronger electron–phonon coupling [10] and the absorption tends to infrared radiation [14] that has been related by the interparticle spacing decrease, which leads to a collective plasmon oscillation of the aggregated system and results in strong dipole–dipole interaction, leading to larger red-shifts of the plasmon mode [10, 11, 16] while for longer spacers the dipolar interaction is very weak or nonexistent and only the plasmon absorbance band is observed in the visible region [12, 17].

In general, the specific geometry of metallic particles usually induces the SPR to exhibit two distinctive bands corresponding to the transverse and longitudinal modes [18]. Au NPs (diameter of 10 nm) showed the presence of a transverse mode at 520 nm, that is shifted to lower wavelengths concerning the plasmon band of spherical particles, albeit by a much smaller amount than the extended plasmon shift, while the extended plasmon (the broad near-IR absorption band) is due to the closely spaced NPs in the aggregate of the gold core NPs [19] or nanoparticle aggregates that arises from strong interparticle interaction [10]. On the other hand, the strong longitudinal band in the near-infrared region [18] is strongly dependent on the aspect ratio [11, 20] or modifying their core and shell molar ratios, and metallic shell thickness [21, 22].

Particularly, in a system formed by a dielectric kernel shelled with small gold crystals, and Au shell thickness increases, a shift of SPR band to the near-infrared regime can be observed [1, 23]. This is often associated with a large dielectric permittivity of the core or can be understood in terms of a plasmon hybridization [24]. Moreover, the plasmon bandwidth becomes broader with a thickness decrease or with an incomplete gold shell formation [1, 9, 14]. Therefore, this type of core–shell structure has gained considerable attention in therapeutic and diagnostic applications that require near-IR absorption, due to the possibility of SPR band tuning by changing the Au shell characteristics [25]. A study demonstrated that by increasing the gold shell thickness, a significant reduction in the applications with a light response is obtained [26].

A common approach for the fabrication of these gold core–shell nanostructures can involve the use of silica (SiO_2) as a core material mainly due to its physical and chemical properties [27, 28], its chemical inertness, and transparency [11]. The assembling normally starts with the synthesis of SiO_2 cores by the Stöber method, followed by its polymer-modified surface such as amine groups to their decorates with a solution of small gold colloid with 1–2 nm in diameter is used as nucleation sites for the reduction and growth of increased coverage of gold on the NPs surface [22] or by the in situ-precipitation method, which is an alternative method that can directly crystallize metallic gold on silica from gold ions solutions (instead AuNPs seeds) [29]. Also, gold ions can be reduced using the leaf extracts (at room temperature) resulting in a 'monodisperse medium' of NPs and biocompatible [30]. Gold NPs synthesized by the citrate reduction method show that by decreasing the molar ratio between citrate and gold during synthesis, the size of the particles is increased, as well as their polydisperse and being less spherical [31]. Gold NPs were stabilized by linking thiol on the surface and the presence of amine/ammonium ending groups, with $NaBH_4$ as the reducing agent [32]. Other synthetic strategies can be used to control the Au shell size assembled into an aggregate structure. Hollow Au nanostructures can be formed by using relatively smaller silver nanospheres as sacrificial templates and ions as the galvanic replacement reagent [33].

The in situ-precipitation method offers the advantage of fewer steps in the synthesis process and minimizing the formation of diversiform or the nucleation of gold crystals out from the silica surface. The formation of this gold shell is directly affected by the attraction strength between the SiO_2 core surface and the gold shell species in the solution, thus its packing density and architecture can be adjusted by modulating the surface potential on the core and shell particles through stringent control of key parameters, e. g. the concentration of Au^{3+} and its mass ratio to the SiO_2 support and reductant, ionic strength, temperature, time, and pH of the reaction. Particularly, the hydrogen ionic potential of the medium can finely alter the ionization of the species in a solution and/or moieties attached to the surface of gold and SiO_2 NPs to optimize the adsorption and subsequent metallization of gold ions on the silica surface. The ionization of species adsorbed on silica surface can also improve the dispersion of SiO_2 NPs, avoiding the formation of multicore structures and allowing the obtention of more homogeneous shells during gold capping [29].

For this purpose, amine-terminated stabilizing agents such as polyethyleneimine (PEI)—which becomes highly positively charged depending on the pH—have been utilized to functionalize SiO_2 NPs before gold coating [25]. In fact, the amine-functionalized silica surface facilitates the adsorption of anionic gold species (such as $AuCl_4^-$) to its further reduction and Au shell growth [29]. However gold cations (e.g. Au^{3+}) are expected to be poorly adsorbed on positively charged PEI-coated SiO_2 NPs to form an Au shell by in situ reductions. Thus, for overcoming this constraint and to obtain gold-shelled SiO_2 NPs from PEI-coated cores and using gold (III) acetate as Au^{3+} source, we propose a simple route of synthesis where a reductant anion (BH_4^-) is prior adsorbed on SiO_2 NPs charged positively, decreasing substantially the superficial charge of silica and allowing the adsorption of Au^{3+} for a further reduction of these ions form a gold shell by the in situ-precipitation method. This is an alternative to the gold-seeding methods and the use of anionic gold species for the core–shell gold/silica NPs obtention with an important red-shift in UV–Vis absorption.

2 Experimental section

2.1 Chemicals

Ammonium hydroxide (25%) was obtained from Acros, tetraethyl orthosilicate (TEOS) (99%), sodium borohydride ($NaBH_4$, 98%), polyethyleneimine branched (PEI, Mw ≈ 25 000 g mol^{-1}) and absolute ethanol were obtained from Sigma-Aldrich. Gold (III) acetate 99.9% was purchased from Alfa Aesar. All chemicals were used as received.

2.2 Synthesis of the PEI-modified silica NPs core

The silica NPs were synthesized following a standard Stöber method that includes hydrolysis and subsequent condensation of tetraethyl orthosilicate (TEOS) in basic conditions [34]. In a typical synthesis, 50 mL absolute ethanol and 3 mL ammonium hydroxide (25% wt in water) were stirred for 5 min. Thus, 1.5 mL of TEOS solution was dropwise added and the mixture was maintained under magnetic stirring for 12 h at room temperature. The resulting precipitate was collected by centrifugation at 3000 rpm for 7 min and washed with ethanol 4 times and finally transferred to an aqueous medium. Then, 0.28 g of PEI (previously dissolved in 50 mL deionized water) was added to the SiO_2 dispersion (8.13 mg/mL) and the mixture was stirred at room temperature for 48 h. The obtained precipitate was washed three times with water to remove the non-attached PEI and the functionalized silica NPs (PEI-SiO_2) were redispersed in deionized water.

2.3 Synthesis of gold-decorated SiO₂ NPs

An amount of metallic gold was deposed on PEI-SiO_2 surface for obtaining Au nanoshell onto SiO_2 system by adapting a method reported in the literature [35]. For this purpose, it is initiated by preparation of 1.0 mg of sodium borohydride ($NaBH_4$) was dissolved in 40 mL water, after adding 1 mL of PEI-SiO_2 NPs suspension (concentration of ~ 8.13 mg/mL). The mixture is kept stirred for 15 min at pH = 7.5. Then, 5 mg of gold (III) acetate (dissolved in 5 mL water that is stirred until the Au ions have been dispersed) was added to the mixture, and the mixture was stirred for 10 min at 500 rpm at room temperature. After that, the Au@PEI-SiO_2 NPs were washed with water several times to remove the excess reactants and finally were redispersed in deionized water and the pH was adjusted to 7.

2.4 Characterization methods

The morphology and size distribution of NPs were characterized by Transmission electron microscopy (TEM) images that were collected with a JEOL JEM 1010 microscope operating at 120 kV. Samples were prepared by placing one drop of a dilute suspension of NPs in the water on a carbon-coated copper grid and air-dried at room temperature. The average particle size and distribution were evaluated by measuring 200 particles. The data were fitted with a lognormal distribution. The X-ray diffraction (XRD) patterns of the samples were obtained using a Rigaku Miniflex 600 diffractometer operating at 30 mA and 40 kV from 20 to 80° (2θ value) using Cu–Kα radiation (0.15418 nm). The samples were prepared by placing a drop of concentrated NPs suspension on a zero-background diffraction silicon sample holder. XRD patterns were analyzed using Rietveld structure refinement. X-Ray photo electron spectroscopy (XPS) was performed using a SPECS Sage HR 100 spectrometer equipped with a hemispherical electron analyzer and monochromatic Al Kα radiation operated of 1486.6 eV energy at 350 W and 10^{-9} mbar. The data were analyzed using the Casas Software (Version 5.921) and peak deconvolution was performed using a 70% Gaussian and 30% Lorentzian line shape with a Shirley nonlinear sigmoid-type baseline. The XPS results were corrected using the C 1s peak (284.6 eV). All measurements were performed on freshly prepared samples to guarantee the reproducibility of the results. The surface charge of samples was measured in a Malvern Zetasizer Nano-ZS90 (Malvern Instruments Ltd., U.K.) at room temperature and samples were dispersed in water at 10 mM of KCl. The pH of aqueous solutions was adjusted by adding 1 mol/1 HCl or 1 mol/L NaOH. To evaluate the optical properties of samples, the measurements were carried out using a JASCO spectrometer (UV-1700) at room temperature. The samples were

diluted in 1 mL water in a standard quartz cuvette used to quantify the light that is absorbed and scattered of the sample.

3 Results and discussion

In order to optimize the silica NPs functionalization with PEI and to improve gold deposition, the pH of dispersions was controlled during synthesis given modifying the NPs surface charge. The surface charge of the NPs was investigated using zeta potential (ζ) measurements. Thus, firstly, the modification of SiO_2 surface by PEI to obtain the PEI-modified SiO_2 NPs, and the pH was fixed in ~ 7.4, where the ζ value of bare silica was − 37.5 mV. The silica isoelectric point was close to pH 2, above which the surface was negatively charged due to the ionized moieties at the SiO_2 surface [36]. After introducing PEI, the ζ values increased to + 27.6 mV (PEI-coated SiO_2), indicating a successful functionalization of the SiO_2 surface with the polymer. At this pH, PEI amine groups are substantially protonated ($-NH_3^+$) and the electrostatic interaction of these moieties with the negatively charged surface of SiO_2 favors the adsorption of PEI. Moreover, the unbound solution-oriented amine groups of adsorbed PEI gave rise to the positive charges on the PEI-SiO_2 surface (see Fig. 1).

In this work, to reduce gold onto PEI-SiO_2 surface, our strategy was firstly adding the reducing agent (BH_4^- ion) instead of the ionic Au^{3+}, as is normally employed in this type of synthesis (with seeds of gold particles of a few nanometers in diameter are prepared [22] and their growth starts in a solution containing a reducing agent and the seed suspension [20] or Au^{3+} ions to the formation of a metal shell [21]). In this case, borohydride anions are electrostatically driven to the positively charged PEI-SiO_2 surface and the surface charge decreases significantly as schematized in Fig. 1. Then, an excess of Au^{3+} can be added to be more easily attracted and reduced onto the PEI-SiO_2 surface which was rich in BH_4^- ions.

Figure 2 shows TEM images with detailed morphology of gold shelled NPs and the histogram of the size distribution of SiO_2 NPs before and after gold coating. The analysis of these histograms indicates the bare SiO_2 core has ~ 75 nm and, after gold capping, the average diameter of the nanostructures increased to ~ 81 nm, resulting in an Au nanoshell thickness of ~ 6 nm. Besides, a close inspection of the TEM image indicates that the Au nanoshell is inhomogeneous and randomly deposited
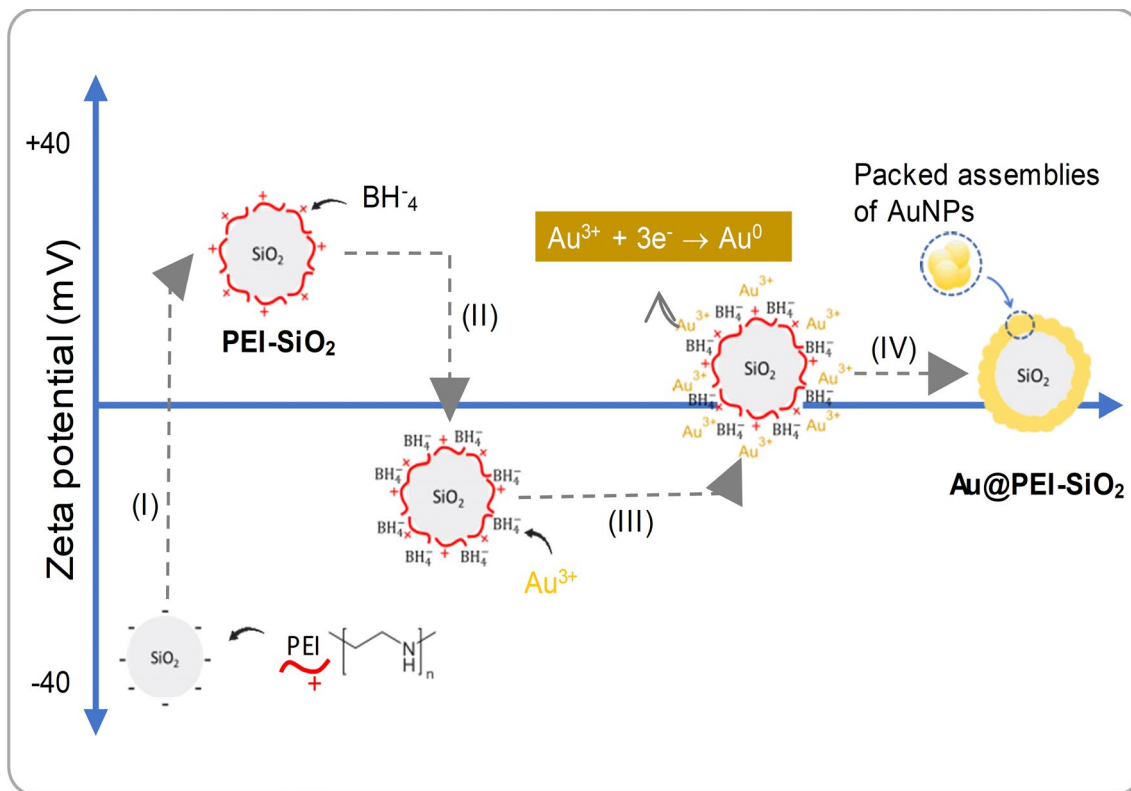

Fig. 1 Schematic representation of synthesis procedure of gold-decorated NPs by in situ-precipitation: **a** Negatively charged SiO_2 NPs are coated with polyethyleneimine (PEI); **b** Positively charged silica NPs (PEI-SiO_2) adsorb BH_4^- reducing anions; **c** Au^{3+} ions are adsorbed on BH_4^- rich SiO_2 surface to be reduced **d** into metallic gold, forming a shell of AuNPs
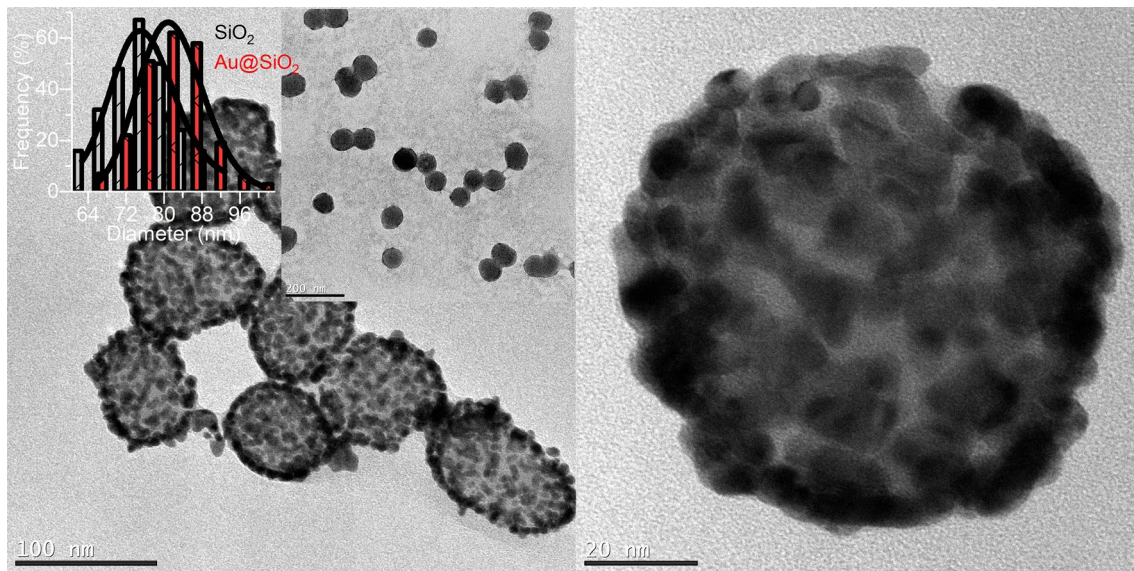
Fig. 2 *Left panel* TEM images of Au@PEI-SiO$_2$ and SiO$_2$ NPs (*right inset*); the *left inset* shows the size histograms using lognormal function of Au@PEI-SiO$_2$ (*red*) and SiO$_2$ (*gray*) NPs. In the *right panel* a single nanoparticle of Au@PEI-SiO$_2$ is showed. *Scale bars* in the inset for *left* and *right* panels are 100 nm and 20 nm, respectively

on SiO$_2$ surface with areas not covered. This could likely do the low concentration BH$_4^-$/Au^{3+} ratio utilized during gold deposition, which can result in small AuNPs forming inhomogeneous aggregates [37] while Chen et al. [38] reported that the formation of Au NPs required a high concentration of NaBH$_4$ that might result in a quick reduction of Au^{3+}, obtaining the formation of small-sized gold NPs. Other researchers reported that the aggregation of Au NPs has been attributed to adding excess NaBH$_4$ [16], suggesting the borohydride favors the formation of a large number of cores and unleashes a disordered growth process leading to polydispersity of size [39]. The increase in the amount of NaBH$_4$ also increases the Au NPs size [40]. All this indicates the formation of Au nanoshell NPs depends on the ratio of the BH$_4^-$/Au^{3+} species. Au shells with similar aspects composed by randomly assembled NPs forming irregular nanochains and/or nanoflower-like crystal structures have been also reported in the literature [41, 42].

In Fig. 3, the main crystalline phase observed is corresponding to the gold cubic structure with space group Fm3m (225) (JCPDS card no. 98-0000230) and a lattice parameter a = 4.187 ± 0.002 Å, determined from Rietveld refinement. Moreover, the broad peak around ~ 19° could be assigned to the amorphous SiO$_2$ phase [43]. The crystallite size of the gold nanoshell can be estimated from the Scherrer equation, expressed as D = Kλ/Γ · $cos\theta_{hk}$, where λ is the incident radiation wavelength, Γ is the diffraction line broadening, θ_{hkl} is Bragg´s angle. For spherical hollow NPs the Scherrer constant can be written as

$$K = \frac{42^{2/3}(\frac{\pi}{3})^{1/3}(t(3R^2-3Rt+t^2))^{4/3}}{3t^2(-6R^2+6Rt-2t^2+(-2R+t)^2Log[\frac{t}{2R-t}])},$$ where R (D = 2R) and t are the particle radius and shell thickness, respectively [44]. Using this formalism and considering R = 81 nm (from TEM analysis) the gold thickness was estimated in ~ 3 nm in good agreement with the Au nanoshell thickness from TEM measurements.

The particle's surface composition was studied by X-ray Photoelectron Spectroscopy (XPS). Figure 4 shows the survey spectra of PEI-SiO$_2$ and Au@PEI-SiO$_2$. The peaks at binding energies (BEs) at ~ 103 eV and ~ 534 eV, corresponding to Si 2p and O 1s, are typical of amorphous silica [45]. Moreover, the peaks at BEs at ~ 285 eV and ~ 399.3 eV, corresponding to C 1s and N 1s, indicate a successful functionalization of SiO$_2$ surface with PEI molecules. The amine groups of N 1s can be bonds with oxygen [46, 47] and it disappears when protonated amine with gold. After Au coating, peaks intensity corresponding to Si 2 s, Si 2p, O 1s, and C 1s cores decreases while for N 1s core, the peak practically disappears, a new peak corresponding to Au 4f appeared. The Si 2p spectrum was fitted with two distinct components at 101.8 eV and 102.9 eV, which could be attributed to Si–N and Si–O–Si bonds respectively, further confirming the presence of NH$_2$ groups onto SiO$_2$ [48]. After Au coating the Si 2p decreased and was fitted with Si–N and Si–OH with BEs of 101.7 eV and 103.2 eV, respectively, this latter was formed due to the electronegativity of silicon atoms with the hydrogen atom [49]. Curves fitting reveal the O 1s peaks at 531.2 and 532.5 eV resulting from Si–O/C-O and Si–O-Si, respectively [47]. After coating

Fig. 3 XRD pattern of Au@PEI-SiO$_2$ sample. The blue line is the difference between the experimental data (*plus marks*) and the calculated curve from Rietveld analysis (*red line*)

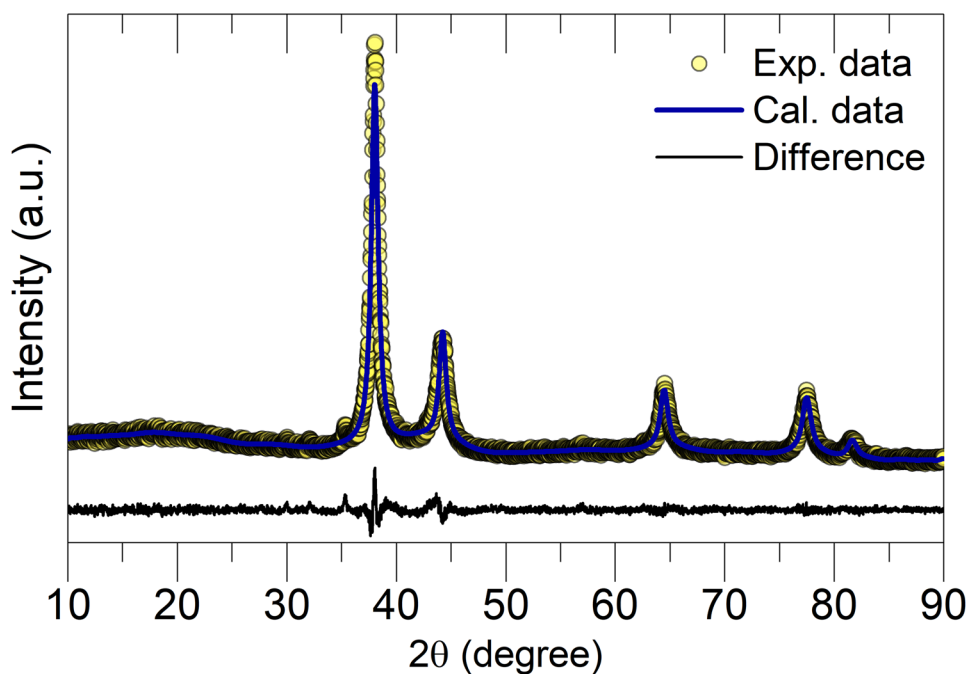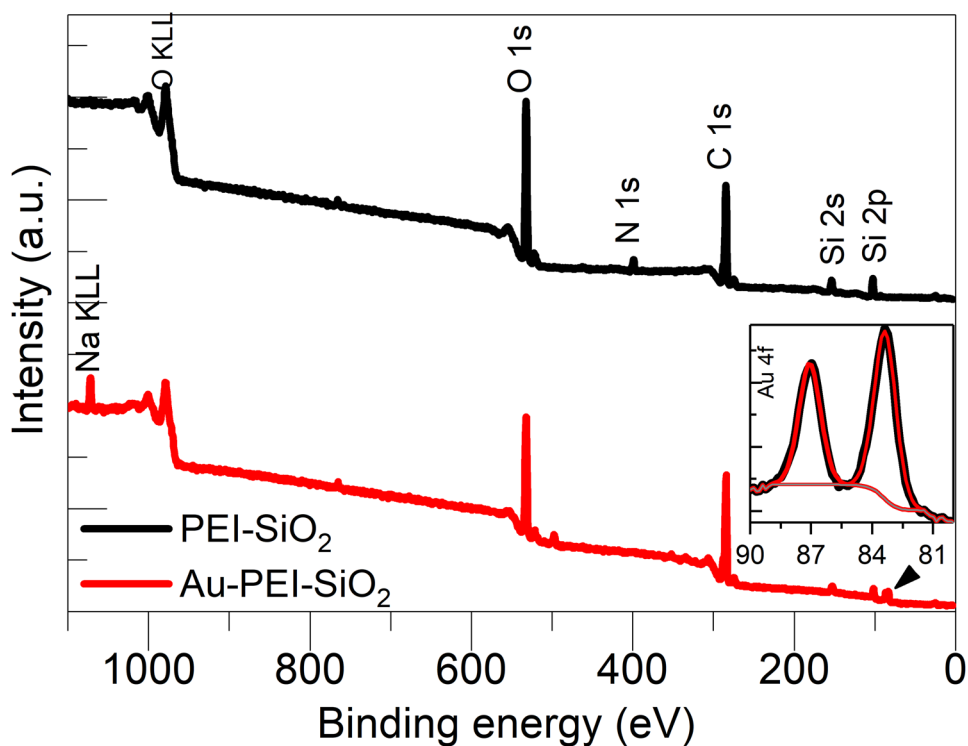**Fig. 4** XPS survey spectra of the PEI-SiO$_2$ and Au@PEI-SiO$_2$ samples. The inset shows the peak fit of the Au 4f core

the O 1s decreased due to the Au NPs attachment on PEI-SiO2 surface, and was fitted with Si–O-Si and Si–OH/C=O with BEs of 532.1 eV and 533.4 eV, respectively [49, 50]. Besides, the weak signal of Si after Au coating could be due to the small thickness of Au nanoshell and/or the presence of exposed areas of PEI-SiO$_2$ surface which were not completely covered with Au. Doublet deconvolution

for the high-resolution Au 4f spectrum (see inset) shows two peaks at 83.4 and 87.1 eV corresponding to Au 4f$_{7/2}$ and Au 4f$_{5/2}$. The 4f doublet splitting (~3.7 eV) indicates Au exits only in its metallic state [51, 52]. The C 1s spectrum was fitted with three components corresponding to C–C/C–H that could be attributed to residual carbon impurities and in part to the C–C of PEI at 284.6 eV, to

C–N bond component could be associated with the of an amine group (–NH) of PEI at 286.1 eV [46, 47, 53], and verify the immobilization of PEI on the SiO2 surface. The highest BE at 288.2 eV is mainly due to the amide group (C=O) and the carboxyl group (O=C–OH) [54] that could be due to an interaction between PEI radicals and water molecules [53]. After coating, C–C/C–H bond persists and the C–N/C–O [55] bond at 286.2 eV, while the variation of C=O/O=C–OH bond was insignificant at 288.5 eV [56]. The presence of C–O/C=O plays a role in Au binding, this mechanism is the same as that suggested in the previous studies. [57]. The residual C 1s signal can be attributed to a possible carbon surface contamination from non-detached PEI as well as from unhydrolyzed TEOS on these exposed areas.

Figure 5 shows SiO$_2$ NPs typical UV–Vis spectra before and after gold-coating. As expected, the PEI-SiO$_2$ NPs did not present any noticeable absorption peak in the investigated wavelength range, whereas Au@PEI-SiO$_2$ NPs exhibited an absorption band at ~680 nm due to surface plasmon resonance (SPR) of gold [57]. A spectrum of spherical AuNPs (diameter ~6 nm) obtained from the same procedure described in the synthesis process, but without adding PEI-SiO$_2$ NPs, is also shown in Fig. 5. This spectrum of spherical solid AuNPs showed a narrower SPR band between ~520 and 531 nm, which is characteristic of

individual gold NPs [12, 57, 58] depending on the polydispersity and size of AuNPs [18].

Besides, the broad aspect of this band and an important red-shift at ~680 nm observed in sample Au@PEI-SiO$_2$ can be associated with the presence of a gold nanoshell forming of small AuNPs aggregates of different sizes, structures, and orientations, or densely packed structures so that the single particles are electronically coupled to each other [10], resulting in interparticle collective interactions due to the decrease of interparticle space among AuNPs [58–60] that contribute the total plasmon band absorption. Bellino et al. [17] reported the absorbance decay is the result of the aggregation of NPs are depending on the number and density of NPs in the aggregates wherein the particles have geometrical arrangements (shapes, sizes) [10]. Meanwhile, Rudoy et al. [21] reported a broad absorption peak for a thickness of 4 nm gold due to the formation of a discontinuous Au shell and its structure is similar to that of an island film. This can be corroborated by the results of TEM which indicate the presence of a nanoshell of inhomogeneous and/or non-uniform AuNPs aggregates [10] structures onto the SiO$_2$ core surface. XRD studies show that the tiny particles (3 nm size) that form part of the packed structures of aggregates.

The presence of small amounts or particle aggregates typically shows strong absorbance at longer wavelengths due to the reduced mean free path of the electrons on the long-wavelength region. From this viewpoint, mean free path corrected Mie theory affords a quantitative description of the absorbance of Au NPs can be determined directly from UV–Vis spectra for the calculation of particle diameter (with an average deviation of ~18% for the calculation of the particle sizes) is given by [61]: $d = \exp\left(3.55\frac{A_{spr}}{A_{450}} - 3.11\right)$, where A_{spr} is the surface plasma resonance peak, and A_{450} is the absorbance at 450 nm. Using the above expression, the calculated diameter was 9.5 ± 1.7 nm. The calculated diameter of the surface plasmon peak helps to acquire a clear insight into particle aggregate size that is a large number of agglomerated atoms [10] that are modeled as being spherical NPs, which is supported by the results of TEM and XRD analysis that indicate the interparticle distance was reduced and NPs start to coalesce and aggregate, with the extent of aggregates, and inhomogeneities in NPs shape and size confirmed the results observed by UV–Vis absorption.

The simple method of synthesis utilized in this work—based on in situ-precipitation—allows the obtention of gold-decorated silica NPs with an important red-shift in SPR wavelength when compared with other elaboration methods, mainly based on gold seeding on silica NPs, which involves more steps for synthesis and less red-shift efficiency. For instance, Daware et. al prepared spherical
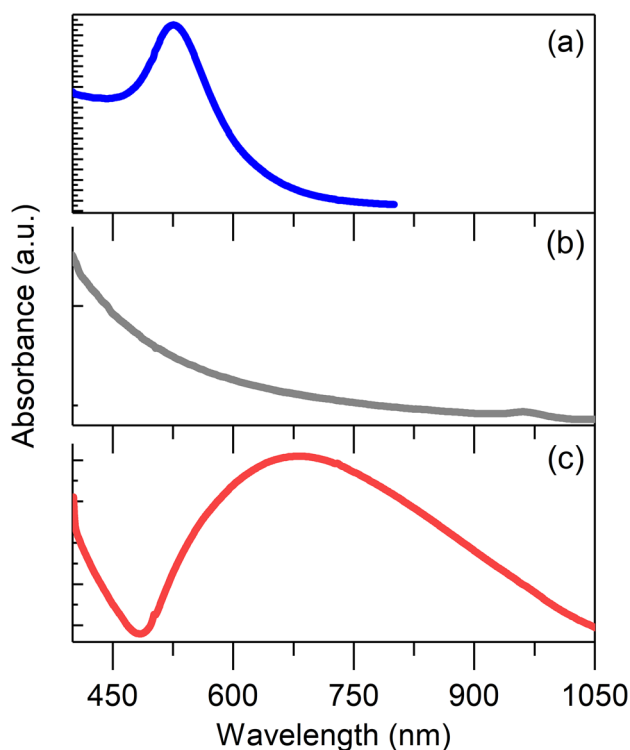
Fig. 5 UV–Visible absorption spectra of **a** gold, **b** PEI-SiO$_2$ and **c** Au@PEI-SiO$_2$ nanoparticles in water solution

silica NPs with an average particle size of 200 nm with AuNPs (~ 8 nm) anchored onto SiO_2 surface. Using a multi-step procedure, SiO_2 was synthesized using a standard Stöber method, and, separately, AuNPs were obtained by the reduction of chloroauric with trisodium citrate and thus were functionalized with polyvinyl pyrrolidone (PVP). The self-assembly of Au and SiO_2 NPs resulted in a system with an SPR peak at 517 nm [57]. Lee et al. prepared a core–shell structure, with an 18 nm magnetic core and SiO_2 shell with a thickness of 40 nm. On silica shell surface, ca. 5.5 nm Au NPs were immobilized acting as the plasmonic substrate. In this case, PVP functionalized magnetite NPs were coated with SiO_2 using an adapted Stöber method. The silica surface was modified with thiol groups using 3-mercaptopropyltriethoxysilane (MPTS). Thus, Au NPs immobilized silica-coated MNPS were selectively collected from the unbounded excess Au NPs by applying a magnetic force. The resulting gold-coated system showed a SPR peak at 530 nm [12]. Abdollahi et al. [14] functionalized SiO_2 NPs (~ 100 nm) with amine groups using 3-aminopropyltriethoxysilane. Thus citrate-functionalized 4.5 nm-sized AuNPs, separately obtained by reduction of $HAuCl_4$ with $NaBH_4$ and trisodium citrate, were attached to the SiO_2 surface. This system showed a SPR peak at 520 nm.

4 Conclusions

In this study, we have succeeded Au-decorated onto SiO_2 surface at room temperature through in-situ precipitation/reduction of Au^{3+} ions onto PEI-functionalized silica NPs rich in reducing BH_4^- ions have proven to be a very simple methodology proposed with appreciable optical properties. This protocol produces a ~ 6-nm thin inhomogeneous aggregates and a randomly deposited layer of AuNPs onto SiO_2 surface with an important red-shift at ~ 670 nm. The plasmon coupling in small AuNPs aggregates, or different orientations of packed assemblies´ structures, with decreased neighboring spacing and strong interparticles interaction, caused a large-shift and a significant dip-up of the Plasmon band, in contrast to that of well-dispersed particles. This could be an alternative to the traditional seeding methods of gold deposition for the obtention of core–shell multifunctional nanoplatforms of importance in potential photothermal treatments and diagnostic applications.

Compliance with ethical standards

References

1. Jin Y, Jia C, Huang S-W et al (2010) Multifunctional nanoparticles as coupled contrast agents. Nat Commun 1:41. https://doi.org/10.1038/ncomms1042
2. Miao Y, Gan N, Li T et al (2016) An ultrasensitive fluorescence aptasensor for chloramphenicol based on FRET between quantum dots as donor and the magnetic SiO2@Au NPs probe as acceptor with exonuclease-assisted target recycling. Sensors Actuators B Chem 222:1066–1072. https://doi.org/10.1016/j.snb.2015.09.049
3. Mao K, Zhou Z, Han S et al (2018) A novel biosensor based on Au@Ag core-shell nanoparticles for sensitive detection of methylamphetamine with surface enhanced Raman scattering. Talanta 190:263–268. https://doi.org/10.1016/j.talanta.2018.07.071
4. Maximenko A, Depciuch J, Łopuszyńska N et al (2020) Fe 3 O 4 @ SiO 2 @Au nanoparticles for MRI-guided chemo/NIR photothermal therapy of cancer cells. RSC Adv 10:26508–26520. https://doi.org/10.1039/D0RA03699D
5. Yang L, Yan Z, Yang L et al (2020) Photothermal conversion of SiO 2 @Au nanoparticles mediated by surface morphology of gold cluster layer. RSC Adv 10:33119–33128. https://doi.org/10.1039/D0RA06278B
6. Wang Y, Barhoumi A, Tong R et al (2018) BaTiO3-core Au-shell nanoparticles for photothermal therapy and bimodal imaging. Acta Biomater 72:287–294. https://doi.org/10.1016/j.actbio.2018.03.029
7. Agabeigi R, Rasta SH, Rahmati-Yamchi M et al (2020) Novel chemo-photothermal therapy in breast cancer using methotrexate-loaded folic acid conjugated Au@SiO2 nanoparticles. Nanoscale Res Lett 15:62. https://doi.org/10.1186/s11671-020-3295-1
8. He Y, Laugesen K, Kamp D et al (2019) Effects and side effects of plasmonic photothermal therapy in brain tissue. Cancer Nanotechnol 10:8. https://doi.org/10.1186/s12645-019-0053-0
9. Lim J, Majetich SA (2013) Composite magnetic–plasmonic nanoparticles for biomedicine: manipulation and imaging. Nano Today 8:98–113. https://doi.org/10.1016/j.nantod.2012.12.010
10. Ghosh SK, Pal T (2007) Interparticle coupling effect on the surface plasmon resonance of gold nanoparticles: from theory to applications. Chem Rev 107:4797–4862. https://doi.org/10.1021/cr0680282

11. Langer J, Novikov SM, Liz-Marzán LM (2015) Sensing using plasmonic nanostructures and nanoparticles. Nanotechnology 26:322001. https://doi.org/10.1088/0957-4484/26/32/322001

12. Lee M, Kang Y-L, Rho W-Y et al (2015) Preparation of plasmonic magnetic nanoparticles and their light scattering properties. RSC Adv 5:21050–21053. https://doi.org/10.1039/C5RA00513B

13. Link S, El-Sayed MA (1999) Size and temperature dependence of the plasmon absorption of colloidal gold nanoparticles. J Phys Chem B 103:4212–4217. https://doi.org/10.1021/jp984796o

14. Abdollahi SN, Naderi M, Amoabediny G (2012) Synthesis and physicochemical characterization of tunable silica–gold nanoshells via seed growth method. Colloids Surf A Physicochem Eng Asp 414:345–351. https://doi.org/10.1016/j.colsurfa.2012.08.043

15. Zhou M, Zeng C, Chen Y et al (2016) Evolution from the plasmon to exciton state in ligand-protected atomically precise gold nanoparticles. Nat Commun 7:13240. https://doi.org/10.1038/ncomms13240

16. Deraedt C, Salmon L, Gatard S et al (2014) Sodium borohydride stabilizes very active gold nanoparticle catalysts. Chem Commun 50:14194–14196. https://doi.org/10.1039/C4CC05946H

17. Bellino MG, Calvo EJ, Gordillo G (2004) Adsorption kinetics of charged thiols on gold nanoparticles. Phys Chem Chem Phys 6:424. https://doi.org/10.1039/b312252b

18. Venditti I (2019) Engineered gold-based nanomaterials: morphologies and functionalities in biomedical applications. A mini review. Bioengineering 6:53. https://doi.org/10.3390/bioengineering6020053

19. Fratoddi I, Cartoni A, Venditti I et al (2018) Gold nanoparticles functionalized by rhodamine B isothiocyanate: a new tool to control plasmonic effects. J Colloid Interface Sci 513:10–19. https://doi.org/10.1016/j.jcis.2017.11.010

20. Alekseeva A V., Bogatyrev VA, Trachuk LA, Khlebtsov NG (2005) Synthesis, fractionation, and optical characterization of Au-Ag composite nanorods. In: Zimnyakov DA (ed). p 18

21. Dement'eva O V., Filippenko MA, Kartseva ME, et al (2012) Synthesis of anisotropic plasmonic nanoparticles with core-shell structure and prospects of their application in laser treatment of tumors. Nanotechnol Russ 7:517–526. https://doi.org/10.1134/S1995078012050035

22. Oldenburg S, Averitt R, Westcott S, Halas N (1998) Nanoengineering of optical resonances. Chem Phys Lett 288:243–247. https://doi.org/10.1016/S0009-2614(98)00277-2

23. Schwartzberg AM, Olson TY, Talley CE, Zhang JZ (2006) Synthesis, characterization, and tunable optical properties of hollow gold nanospheres. J Phys Chem B 110:19935–19944. https://doi.org/10.1021/jp062136a

24. Levin CS, Hofmann C, Ali TA et al (2009) Magnetic–plasmonic core–shell nanoparticles. ACS Nano 3:1379–1388. https://doi.org/10.1021/nn900118a

25. Sadtler B, Wei A (2002) Spherical ensembles of gold nanoparticles on silica: electrostatic and size effects. Chem Commun 7:1604 1605. https://doi.org/10.1039/b204760h

26. Brennan G, Bergamino S, Pescio M et al (2020) The effects of a varied gold shell thickness on iron oxide nanoparticle cores in magnetic manipulation, T1 and T2 MRI contrasting, and magnetic hyperthermia. Nanomaterials 10:2424. https://doi.org/10.3390/nano10122424

27. Croissant JG, Fatieiev Y, Almalik A, Khashab NM (2018) Mesoporous silica and organosilica nanoparticles: physical chemistry, biosafety, delivery strategies, and biomedical applications. Adv Healthc Mater 7:1700831. https://doi.org/10.1002/adhm.201700831

28. Yang S-A, Choi S, Jeon SM, Yu J (2018) Silica nanoparticle stability in biological media revisited. Sci Rep 8:185. https://doi.org/10.1038/s41598-017-18502-8

29. Phonthammachai N, Kah JCY, Jun G et al (2008) Synthesis of contiguous silica–gold core–shell structures: critical parameters and processes. Langmuir 24:5109–5112. https://doi.org/10.1021/la703580r

30. Aljabali A, Akkam Y, Al Zoubi M et al (2018) Synthesis of gold nanoparticles using leaf extract of *Ziziphus zizyphus* and their antimicrobial activity. Nanomaterials 8:174. https://doi.org/10.3390/nano8030174

31. Dong J, Carpinone PL, Pyrgiotakis G et al (2020) Synthesis of Precision Gold Nanoparticles Using Turkevich Method. KONA Powder Part J 37:224–232. https://doi.org/10.14356/kona.2020011

32. Venditti I, Testa G, Sciubba F et al (2017) Hydrophilic metal nanoparticles functionalized by 2-diethylaminoethanethiol: a close look at the metal-ligand interaction and interface chemical structure. J Phys Chem C 121:8002–8013. https://doi.org/10.1021/acs.jpcc.7b01424

33. Choi Y, Hong S, Liu L et al (2012) Galvanically replaced hollow Au–Ag nanospheres: study of their surface plasmon resonance. Langmuir 28:6670–6676. https://doi.org/10.1021/la202569q

34. Masalov VM, Sukhinina NS, Kudrenko EA, Emelchenko GA (2011) Mechanism of formation and nanostructure of Stöber silica particles. Nanotechnology 22:275718. https://doi.org/10.1088/0957-4484/22/27/275718

35. León Félix L, Sanz B, Sebastián V et al (2019) Gold-decorated magnetic nanoparticles design for hyperthermia applications and as a potential platform for their surface-functionalization. Sci Rep 9:4185. https://doi.org/10.1038/s41598-019-40769-2

36. Wu S-H, Mou C-Y, Lin H-P (2013) Synthesis of mesoporous silica nanoparticles. Chem Soc Rev 42:3862. https://doi.org/10.1039/c3cs35405a

37. Jankiewicz BJ, Jamiola D, Choma J, Jaroniec M (2012) Silica–metal core–shell nanostructures. Adv Colloid Interface Sci 170:28–47. https://doi.org/10.1016/j.cis.2011.11.002

38. Chen G, Takezawa M, Kawazoe N, Tateishi T (2008) Preparation of cationic gold nanoparticles for gene delivery. Open Biotechnol J 2:152–156. https://doi.org/10.2174/1874070700802020152

39. Oliveira JP, Prado AR, Keijok WJ et al (2020) A helpful method for controlled synthesis of monodisperse gold nanoparticles through response surface modeling. Arab J Chem 13:216–226. https://doi.org/10.1016/j.arabjc.2017.04.003

40. Lin C, Tao K, Hua D et al (2013) Size effect of gold nanoparticles in catalytic reduction of p-nitrophenol with NaBH4. Molecules 18:12609–12620. https://doi.org/10.3390/molecules181012609

41. Li L, Weng J (2010) Enzymatic synthesis of gold nanoflowers with trypsin. Nanotechnology 21:305603. https://doi.org/10.1088/0957-4484/21/30/305603

42. Xu D, Gu J, Wang W et al (2010) Development of chitosan-coated gold nanoflowers as SERS-active probes. Nanotechnology 21:375101. https://doi.org/10.1088/0957-4484/21/37/375101

43. Yao Q, Lu Z-H, Zhang Z et al (2015) One-pot synthesis of coreshell Cu@SiO2 nanospheres and their catalysis for hydrolytic dehydrogenation of ammonia borane and hydrazine borane. Sci Rep 4:7597. https://doi.org/10.1038/srep07597

44. Burresi E, Tapfer L (2019) Diffraction line profiles of spherical hollow nanocrystals. Nanomater Nanotechnol 9:184798041983238. https://doi.org/10.1177/1847980419832386

45. Wang X, Masse S, Laurent G et al (2015) Impact of polyethylenimine conjugation mode on the cell transfection efficiency of silica nanovectors. Langmuir 31:11078–11085. https://doi.org/10.1021/acs.langmuir.5b02616

46. Choi K, Lee S, Park JO et al (2018) Chromium removal from aqueous solution by a PEI-silica nanocomposite. Sci Rep 8:1438. https://doi.org/10.1038/s41598-018-20017-9

47. Soulé S, Allouche J, Dupin J-C et al (2015) Thermoresponsive gold nanoshell@mesoporous silica nano-assemblies: an XPS/NMR survey. Phys Chem Chem Phys 17:28719–28728. https://doi.org/10.1039/C5CP04491J

48. Ching JY, Huang BJ, Hsu Y-T, Khung YL (2020) Anti-adhesion behavior from ring-strain amine cyclic monolayers grafted on silicon (111) surfaces. Sci Rep 10:8758. https://doi.org/10.1038/s41598-020-65710-w

49. Simonsen ME, Sønderby C, Li Z, Søgaard EG (2009) XPS and FT-IR investigation of silicate polymers. J Mater Sci 44:2079–2088. https://doi.org/10.1007/s10853-009-3270-9

50. Paparazzo E (1996) On the XPS analysis of Si–OH groups at the surface of silica. Surf Interface Anal 24:729–730. https://doi.org/10.1002/(SICI)1096-9918(19960930)24:10%3c729::AID-SIA183%3e3.0.CO;2-P

51. Yi C-W, Luo K, Wei T, Goodman DW (2005) The composition and structure of Pd–Au surfaces. J Phys Chem B 109:18535–18540. https://doi.org/10.1021/jp053515r

52. Gross T, Ramm M, Sonntag H et al (1992) An XPS analysis of different SiO2 modifications employing a C 1s as well as an Au 4f7/2 static charge reference. Surf Interface Anal 18:59–64. https://doi.org/10.1002/sia.740180110

53. Yun H-J, Hong H, Lee J, Choi C-J (2014) Chemical and structural properties of polyethyleneimine film coated on a SiO$_2$ substrate in different concentrations. Mater Trans 55:801–805. https://doi.org/10.2320/matertrans.M2014013

54. Zhang Z, Wu Y (2010) Investigation of the NaBH 4-induced aggregation of Au nanoparticles. Langmuir 26:9214–9223. https://doi.org/10.1021/la904410f

55. Zhang Z, Jia J, Lai Y et al (2010) Conjugating folic acid to gold nanoparticles through glutathione for targeting and detecting cancer cells. Bioorg Med Chem 18:5528–5534. https://doi.org/10.1016/j.bmc.2010.06.045

56. Allouche J, Soulé S, Dupin J-C et al (2014) Design of gold nanoshells via a gelatin-mediated self-assembly of gold nanoparticles on silica cores. RSC Adv 4:63234–63237. https://doi.org/10.1039/C4RA13793K

57. Daware K, Kasture M, Kalubarme R et al (2019) Detection of toxic metal ions Pb2+ in water using SiO$_2$@Au core-shell nanostructures: a simple technique for water quality monitoring. Chem Phys Lett 732:136635. https://doi.org/10.1016/j.cplett.2019.136635

58. Zhong Z, Patskovskyy S, Bouvrette P et al (2004) The surface chemistry of Au colloids and their interactions with functional amino acids. J Phys Chem B 108:4046–4052. https://doi.org/10.1021/jp037056a

59. Cheng W, Dong S, Wang E (2005) Spontaneous fractal aggregation of gold nanoparticles and controlled generation of aggregate-based fractal networks at air/water interface. J Phys Chem B 109:19213–19218. https://doi.org/10.1021/jp052255a

60. Peng Z, Walther T, Kleinermanns K (2005) Influence of intense pulsed laser irradiation on optical and morphological properties of gold nanoparticle aggregates produced by surface acid–base reactions. Langmuir 21:4249–4253. https://doi.org/10.1021/la047272q

61. Haiss W, Thanh NTK, Aveyard J, Fernig DG (2007) Determination of size and concentration of gold nanoparticles from UV–Vis spectra. Anal Chem 79:4215–4221. https://doi.org/10.1021/ac0702084

Publisher's Note Springer Nature remains neutral with regard to jurisdictional claims in published maps and institutional affiliations.